Geochemical mapping of a paleo-subduction zone beneath the Troodos Ophiolite

Woelki, Dominic

2019-09-30

Woelki , D , Regelous , M , Haase , K M & Beier , C 2019 , ' Geochemical mapping of a paleo-subduction zone beneath the Troodos Ophiolite ' , Chemical Geology , vol. 523 , pp. 1-8 . https://doi.org/10.1016/j.chemgeo.2019.05.041

http://hdl.handle.net/10138/330647
https://doi.org/10.1016/j.chemgeo.2019.05.041

Geochemical mapping of a paleo-subduction zone beneath the Troodos Ophiolite

***Dominic Woelki[1], Marcel Regelous[1], Karsten M. Haase[1], Christoph Beier[1]**

[1]GeoZentrum Nordbayern, Friedrich-Alexander-Universität (FAU) Erlangen-Nürnberg, Schlossgarten 5, D-91054 Erlangen, Germany, dominic.woelki@fau.de

ABSTRACT

Supra-subduction zone ophiolites such as the Cretaceous Troodos Ophiolite of Cyprus are fragments of oceanic crust formed by seafloor spreading close to subduction zones. Their exact tectonic setting of origin has been intensively debated. Although many supra-subduction zone ophiolites are thought to represent fore-arc crust, created during subduction initiation, others may have formed at a subducting ridge, or in a back-arc, ridge-trench-trench/transform triple junction or 'plate edge' setting. We carried out major and trace element analyses of 515 fresh volcanic glasses from 7 detailed sections through the Troodos lava sequence in order to determine the regional and temporal variation in the composition of Troodos magmatism, and hence reconstruct the distance and orientation of the Troodos spreading axis relative to the former subduction zone. Troodos glasses range from boninite through tholeiitic basalt and andesite to dacite. All glasses are enriched in fluid-mobile trace elements, and variably depleted in the high-field strength elements compared to Mid-Ocean Ridge Basalt (MORB). None of these glasses therefore have compositions identical to Izu-Bonin-Mariana fore-arc lavas that have been proposed to be the prime example of lavas formed during subduction initiation. Boninites are apparently restricted to the southern margin of the Troodos Ophiolite, and glasses from the southeast margin of the ophiolite are the most depleted and contain the strongest input

of subduction zone fluid and melt signature. These geographic variations in glass composition indicate that the Troodos Ophiolite formed by NW-SE directed spreading (at 91 Ma) approximately 100 - 120 km above an eastward-dipping subducting plate. The orientation of the Troodos spreading axis relative to the former trench could be explained if the Troodos Ophiolite formed in a fore-arc position by subduction initiation at a transform fault. However, the lack of glasses with fore-arc basalt composition, and similarities between the trace element compositions of Troodos glasses and those from the Fonualei basin and northern Lau Basin in the southwest Pacific suggest that the Troodos Ophiolite formed in a ridge-trench-trench or ridge-trench-transform triple junction setting, at a back-arc spreading centre that propagated into arc and fore-arc crust.

1. Introduction

Ophiolites yield important information on the structure and composition of the oceanic crust and also provide insight into the evolution of large-scale plate tectonic processes. The presence of a sheeted dyke complex, and the similarity to rock types dredged from the oceanic crust implies that ophiolites were formed at oceanic spreading centres (Gass, 1968; Moores and Vine, 1971). The geochemical compositions of lavas from ophiolites show that many formed close to former subduction zones (Miyashiro, 1974; Pearce, 1975; Rautenschlein et al., 1985), but the exact tectonic setting of formation of these 'supra-subduction zone' (SSZ) ophiolites is debated. The presence of boninite lavas in some SSZ ophiolites has led to the perception that they may represent slices of fore-arc crust and since fore-arc crust is thought to have formed during subduction initiation, many SSZ ophiolites are assumed to record subduction initiation

events (Dilek and Furnes, 2009; Ishizuka et al., 2006; Pearce et al., 1984; Reagan et al., 2010; Stern et al., 2012).

The lavas of the Cretaceous (approximately 91 Ma; (Mukasa and Ludden, 1987) Troodos Ophiolite of Cyprus have been divided into an upper and lower pillow lava series, with boninitic lavas apparently restricted to the upper pillow series (Pearce and Robinson, 2010). This stratigraphic association of rock-types is thought to resemble that of the Izu-Bonin-Mariana (IBM) fore-arc, where early fore-arc basalts are overlain by boninites, island arc tholeiitic lavas and calc-alkaline arc deposits, recording the evolution from early spreading during subduction initiation to a mature island arc (Ishizuka et al., 2014; Reagan et al., 2010). However, Woelki et al. (2018) showed that on the southern margin of the Troodos Ophiolite, boninitic and tholeiitic glasses are interbedded with no systematic change in composition with time. Other tectonic models for the origin of the Troodos Ophiolite include formation at a subducting spreading ridge (Osozawa et al., 2012), ridge-trench-trench or ridge-trench-transform triple junction (Regelous et al., 2014; Woelki et al., 2018), rifted arc (Flower and Levine, 1987), or subduction initiation plate edge setting (Pearce and Robinson, 2010). Distinguishing between these various models requires a better understanding of the position of the former Troodos spreading axis to the neighboring trench, and the temporal geochemical evolution of Troodos magmatism. Here, we use geochemical data for lavas from stratigraphic sections through different parts of the ophiolite to reconstruct the position of the ophiolite crust relative to the subducting slab.

2. Samples and analytical methods

In order to determine the spatial relationship between the former Troodos spreading centre and the subduction zone, we examined the geographic and temporal variations in the

composition of lavas from the extrusive section of the Troodos Ophiolite. Hydrothermal alteration of Troodos volcanic rocks has affected the concentrations of many of the fluid-mobile trace elements that are distinctive of subduction-related lavas, however the chemical effects of alteration on bulk lava compositions can be avoided by analysis of fresh volcanic glass using microanalytical techniques. We measured the major and trace element compositions of 515 fresh volcanic glasses, taken largely from seven detailed sections through the volcanic extrusive sequence on both, the northern and southern margins of the ophiolite (Fig. 1, Table S1). These sections cover much of the exposed volcanic extrusive series, and although the sections are not entirely complete where fresh glass is lacking, most cover much of the 1000 - 1500 m thick extrusive section (Figs. 1, 4). By analogy with fast-spreading oceanic crust (Brandl et al., 2016), the period of time recorded in each volcanic section may be between 50 to 100 ky. Structural orientations of the Troodos sheeted dykes are N-S to NW-SE (Maffione et al., 2017), thus lavas from the northern and southern margins of the Troodos Ophiolite are of approximately the same age, and all likely formed over a period of less than 2 My.

Glass samples were crushed and single 1-2 mm sized chips were hand-picked, cleaned in distilled water, embedded in epoxy resin and polished for electron microprobe and laser-ablation ICP-MS analyses. Fresh glasses (n = 515) from seven sections were analysed for major elements, and 270 representative samples were selected for trace element analysis. Analysis of the major elements (SiO_2, TiO_2, Al_2O_3, FeO_t, MnO, CaO, Na_2O, K_2O, P_2O_5 SO_3 and Cl) was carried out using a JEOL JXA-8200 Superprobe electron microprobe at the GeoZentrum Nordbayern (GZN), Friedrich-Alexander Universität Erlangen-Nürnberg, Germany. The microprobe was operated with an acceleration voltage of 15 kV, a beam current of 15 nA and a defocused (10 μm) beam. Counting times were set to 20 s and 10 s for peaks and backgrounds for all elements,

except for Cl where peak counting time was 40 s and background times were set to 20 s. Accuracy and precision were determined using international glass standards VG-2 and VG-A99 measured during each analytical session (Brandl et al., 2012). For the VG-A99 standard, accuracy is better than 7.4 % for all elements except Cl, SO_3, and P_2O_5, and precision is better than 4.7 % except for Cl, SO_3 and P_2O_5 (Beier et al., 2018). The average values of 10 spot analyses on each sample are presented in Table S1.

Trace element concentrations of the glasses were determined by laser ablation inductively coupled plasma mass spectrometry on the same glass fragments analysed for major elements, using an Agilent 7500i quadrupole mass spectrometer coupled with a New Wave Research UP193FX excimer laser at the GeoZentrum Nordbayern. A subset (n = 178) of the samples was measured with a Teledyne Photon Machines Analyte Excite 193nm laser ablation system. The beam diameter was set to 35 - 50 μm and the SiO_2 contents, previously determined by electron microprobe, were used as internal standard. External calibration was performed using the NIST614 glass standard. The international rock standard BCR-2g was measured to determine accuracy and reproducibility. Accuracy was better than 13.1% except for Zn and Cu and precision was better than 9.4% except for As and Cr. Repeat measurement of samples (n = 4) with the newly established New Wave Research UP193FX excimer laser and the Teledyne Photon Machines Analyte Excite 193nm laser yielded comparable values. Data in Table S1 represent averages of four individual analyses of each sample or standard. The new data presented here are combined with published major and trace element data for Troodos glasses from Akaki Canyon (Regelous et al., 2014) and Parekklisia (Woelki et al., 2018) which were measured in the same laboratory.

3. Results

Troodos volcanic glasses range in composition from high-Ca (CaO/Al_2O_3 >0.75) (Crawford et al., 1989) boninite (n=142), through tholeiitic basalt and andesite to dacite (n=373). The MgO and TiO_2 contents of the glasses range from 10.7 to 0.3 wt% and 0.2 to 1.7 wt%, respectively (Fig. 2). True boninitic glasses (with TiO_2 <0.5 wt%, SiO_2 >52 wt% and MgO >8 wt%) occur exclusively on the southern margin of the ophiolite, but are not restricted to the youngest part of the stratigraphy (Fig. 2, 4; Wölki et al., 2018). Highly evolved glasses with MgO <2 wt% were found only on the northern margin (Akaki, Peristerona and Kato Pyrgos) (Fig. 2). The major element variations within glasses from individual sections are broadly consistent with fractional crystallisation of olivine, olivine and clinopyroxene, or clinopyroxene and plagioclase, which occur as microphenocrysts in the glasses. Incompatible trace element ratios do not vary systematically with degree of magma differentiation, indicating that source variations, rather than crystal fractionation or crustal assimilation are responsible for the range in Troodos glass compositions (Fig. S1; König et al., 2010; Regelous et al., 2014; Woelki et al., 2018).

Compared to MORB, most Troodos glasses were derived from more depleted mantle sources (lower Zr/Yb). Ba/Th ratios of Troodos glasses are higher compared to MORB and range from 78 to 270, overlapping with the composition of back-arc lavas from the Eastern Lau and Fonualei Spreading Centres (Bézos et al., 2009; Escrig et al., 2012). All Troodos glasses have relatively high concentrations of the fluid-mobile elements (Cs, Rb, Ba, U, Pb, Sr), with Ce/Pb ratios (0.6 – 8.8) characteristic of subduction-related lavas (Fig. 3, 5). Correlations between fluid-mobile and fluid-immobile trace element ratios (e.g. Ce/Pb and Zr/Yb) for glasses from individual sections indicate that alteration has not affected the compositions of these samples

(Fig. 5). The mantle sources of the boninites and most depleted tholeiitic glasses have also been enriched in Nb and Th by small-degree melts (König et al., 2010; Regelous et al., 2014; Woelki et al., 2018) and display spoon-shaped rare-earth element patterns with La and Ce enrichments. A detailed discussion of the petrogenesis of the Troodos glasses can be found in previous studies (König et al., 2010; Osozawa et al., 2012; Rautenschlein et al., 1985; Regelous et al., 2014; Woelki et al., 2018); here we focus on the stratigraphic and geographic variations in Troodos glass compositions, and their significance in understanding the orientation of the former subduction zone and the tectonic setting of ophiolite formation.

Despite the wide range in composition of Troodos glasses, the sections through the lavas display no systematic change in composition with depth within the lava stratigraphy (Fig. 4). Instead, our data show that the geochemical variations within Troodos glasses are primarily related to their geographical location (Fig. 4, 5) rather than to relative stratigraphic age. Based on trace element geochemistry, we divided the Troodos glasses into three major regions, the northern margin (NM), the south-western margin (SWM), and the south-eastern margin (SEM; Fig. 1). Glasses from the NM have relatively high and uniform Zr/Yb ratios (Fig. 4), whereas those from the SWM are more depleted (lower Zr/Yb), and display a stronger fluid input, with lower Ce/Pb and higher Ba/Ce ratios (see Fig. 4). The most depleted glasses are boninites and tholeiites from the SEM in the vicinity of the Arakapas Transform Fault.

4. Discussion

4.1. Comparison with fore-arc and back-arc lavas

The lack of any systematic change in composition with relative stratigraphic age within the Troodos lava pile contrasts with the geochemical evolution observed in the IBM fore-arc,

where the earliest lavas are fore-arc basalts which formed at short-lived spreading centres during subduction initiation (Reagan et al., 2010) with no or minor subduction input (e.g., high Ce/Pb ratios, Fig. 5). In the IBM fore-arc, the lavas become more depleted in high-field strength elements and more enriched in light rare earth elements and fluid-mobile elements as subduction proceeds. These intermediate lavas are typically overlain by boninites which record the highest degree of mantle wedge depletion and enrichment by subduction zone components (Ishizuka et al., 2018; Ishizuka et al., 2014; Reagan et al., 2010; Reagan et al., 2017; Whattam and Stern, 2011). In contrast, none of our sections through the Troodos lavas exhibits a trend to more depleted, more fluid-enriched compositions with time. More recent drilling of the IBM fore-arc indicates that boninites may in fact be restricted to the shallower side of the fore-arc, with fore-arc basalts located closer to the trench (Pearce et al., 2015). However, in Troodos there are no glasses with Ce/Pb ratios >8 that characterise many fore-arc basalts (Fig. 5), and most Troodos glasses were derived from a highly depleted mantle source (low Zr/Yb), suggesting that the subduction zone existed during the entire spreading stage exposed in the Troodos Ophiolite. Low-Ca boninites from the IBM fore-arc have high Zr and Hf concentrations relative to Sm and Eu (Fig. 3), unlike the high-Ca boninitic glasses from the Troodos Ophiolite. High-Ca boninites without the association of low-Ca boninites are known from the northern termination of the Tonga trench and the southern termination of the Vanuatu Trench (Danyushevsky et al., 1995; Falloon et al., 1987; Sharaskin et al., 1983; Sigurdsson et al., 1993). These two areas represent special tectonic settings where the trench terminates into a transition zone of transform tectonics, and a back-arc spreading centre propagates into the fore-arc region, respectively (Falloon and Crawford, 1991; Sigurdsson et al., 1993).

The compositional range of the lavas and the magmatic evolution of the Troodos Ophiolite is thus very different from that inferred for the IBM fore-arc crust.

Instead, the variably depleted and fluid-mobile element enriched compositions of Troodos glasses are similar to those recovered from back-arc and rear-arc spreading centres. In Fig. 5 and 6, we compare the compositions of Troodos glasses with those from active spreading centres in the Tonga arc - Lau back-arc basin in the western Pacific, which are located at varying distance to the active Tonga arc, and from which fresh volcanic glasses have been recovered (Bach et al., 1998; Bézos et al., 2009; Caulfield et al., 2012a; Escrig et al., 2012; Keller et al., 2008; Pearce et al., 1994; Peate et al., 2001).

In Fig. 5 the NM glasses lie on an array between MORB compositions and arc front lavas from Tofua Island, overlapping with back-arc basin basalts of the Fonualei Spreading Centre (FSC) in the Lau Basin (Fig. 5). The more depleted SWM glasses partly overlap with arc lavas of Tofua Island but extend to lower Zr/Yb and Ce/Pb, indicating higher degrees of mantle depletion and high addition of subduction zone fluid. The SEM glasses are less enriched in fluid-mobile elements but were derived from a depleted mantle source, and overlap in composition with Tonga arc boninites (Fig. 5). The mean composition of 142 Troodos boninitic glasses is similar in composition to young boninites recovered from the Tonga arc and rear-arc (Cooper et al., 2010; Falloon and Crawford, 1991; Falloon et al., 2008; Falloon et al., 2007; Falloon et al., 1989) (Fig. 3). In conclusion, the Troodos glasses have more similarities with Tonga back-arc lavas, than to lavas found in the IBM fore-arc crust.

4.2. Geochemical mapping of the former subduction zone

Previous studies have shown that within the Lau Basin, back-arc lava compositions vary systematically with distance to the active arc front (Bach et al., 1998; Bézos et al., 2009; Escrig et al., 2012; Keller et al., 2008; Pearce et al., 1994; Peate et al., 2001). The geographic variations in Troodos glass compositions and their geochemical similarities to lavas from the active Tonga-Lau subduction system therefore allow us to reconstruct the location and orientation of the former subduction zone beneath the Troodos Ophiolite.

The more depleted and greater fluid enrichment of the glasses from the southern margin of the Troodos Ophiolite indicate that at 91 Ma, the southern section of the Troodos spreading centre was located closer to the trench. The absolute distance from the trench can be estimated by comparison with lavas from spreading centres in the active Tonga – Lau Basin arc – back-arc system. The overlap in composition between the NM glasses and the back-arc lavas from the Fonualei Spreading Centre suggests that ~91 Ma ago the northern margin of Troodos may have been located at a similar distance above the subducting slab as the recent Fonualei Spreading Centre (Fig. 5, 6). The lavas of the Fonualei Spreading Centre erupted close (25 – 75 km) to the active Tofua arc, 175 – 225 km from the Tonga trench, and approximately 125 – 177 km above the subducting slab (Caulfield et al., 2012a; Escrig et al., 2012; Keller et al., 2008). The SEM and SWM glasses were therefore located 30 – 40 km closer to the trench, in an arc or fore-arc position, and by analogy with modern arcs, approximately 100 - 110 km above the subducting plate (Syracuse and Abers, 2006). The very low Zr/Yb ratios of the Troodos SEM and SWM glasses, which are unlike any modern Tonga-Lau or IBM fore-arc lavas, can be explained by the location of the spreading centre in an arc or fore-arc position (Fig. 6), underlain by mantle which was highly depleted by previous melting events, together with high degrees of melting due to

upwelling and melting of hydrous mantle at shallow levels beneath the spreading centre (Flower and Levine, 1987; Moores et al., 1984). In such a position, the arc magmatism would be captured by the overlying spreading centre. The distribution of Troodos glasses in the Fe_8 – Ti_8 diagram (Fig. 7) supports this interpretation. NM glasses (e.g. Akaki) define positive arrays in this diagram, overlapping with back-arc basin basalts of the Eastern Lau Spreading Centre but extending to more depleted (lower Fe_8 and Ti_8) values, consistent with mixing of melts from 'wet' and 'damp' moderately depleted mantle sources (Le Voci et al., 2014). SEM and SWM glasses were derived from depleted and highly depleted wet mantle sources and overlap with Fonualei back-arc lavas (Fig. 7). In conclusion, the Troodos glasses display a greater mantle wedge depletion and higher input of a subduction zone component from north to south, indicating a closer position for the SWM and SEM glasses to the trench.

The Troodos Ophiolite has been rotated 90° anticlockwise since its formation (Clube et al., 1985), thus we infer that at 91 Ma, the Troodos spreading axis was located about 100 – 120 km above an eastward dipping subducting plate (Fig. 8) within the former Tethys Ocean. The relatively high (approximately 45°) angle between the former trench (N-S, as determined from our analyses), and the Cretaceous paleo-spreading axis (E-W to NE-SW, on the basis of sheeted dyke orientations (Maffione et al., 2017), may explain the steep along-axis geochemical gradients observed in the Troodos glasses.

4.3. Geodynamic setting of formation of the Troodos Ophiolite

Our major and trace element data, in particular the enrichment in fluid-soluble elements (Rb, Cs, U, Pb, Ba) for fresh, unaltered volcanic glasses from the Troodos Ophiolite confirm its formation in a "supra-subduction zone" setting, as previously reported by many workers (Pearce

and Robinson, 2010; Rautenschlein et al., 1985; Regelous et al., 2014; Robinson et al., 2003; Robinson et al., 1983; Woelki et al., 2018). The more depleted trace element compositions, lower Ce/Pb and the presence of boninites suggest that the Troodos spreading axis was located closer to the trench than most currently-active back-arc spreading centres, in an arc or fore-arc position.

In many models of subduction initiation, the spreading centres at which fore-arc crust was accreted are presumed to have been oriented parallel to the trench (Pearce et al., 2015). The high angle between the former trench and the Troodos spreading axis inferred from our data is incompatible with such a model, but could possibly be explained by models of subduction initiation in which a trench initiates within oceanic crust at a transform fault (e.g. (Casey and Dewey, 1984). However, as discussed above, fluid-enriched compositions of all Troodos glasses and the extremely low Zr/Yb in the most depleted glasses suggest that the Troodos crust formed above an existing subduction zone, rather than during subduction initiation.

The geometry we infer for the former Troodos ridge-trench system is also inconsistent with some previous models for the geodynamic setting of the Troodos Ophiolite. Osozawa et al. (2012) argued for ridge subduction shortly after subduction initiation. However, the depleted compositions of Troodos glasses, with Zr/Yb < MORB and higher contribution of a slab component (Ce/Pb <10) , are unlike those from the subducting segments of the Chile Rise closest to the South American Trench (Ce/Pb >16) (Karsten et al., 1996). As previously suggested (Flower and Levine, 1987; Moores et al., 1984; Regelous et al., 2014; Woelki et al., 2018), we conclude that the Troodos Ophiolite formed at a ridge-trench-trench (RTT) or ridge-trench-transform (RTF) triple junction, where previously depleted, fluid-enriched mantle above the subducting slab underwent extensive melting beneath the spreading axis. This setting is similar

to the trench-transform 'plate-edge' setting of Pearce and Robinson (2010), but without appealing to subduction initiation.

Such tectonic settings are rare on Earth today, but present-day equivalents may include the southern North Fiji Basin (intersection of the Central North Fiji Basin spreading centre with the Hunter Fracture Zone and the Southern Vanuatu Trench) and the northern Tonga Arc – Lau Basin (intersection of the Northeast Lau Spreading Centre and the Vitiaz – Tonga Trench). In both locations, young, predominantly high-Ca boninites have been reported (Crawford et al., 1981; Crawford et al., 1989; Danyushevsky et al., 1995; Resing et al., 2011; Sigurdsson et al., 1993), which are unrelated to subduction initiation. Upwelling of previously-depleted, fluid-enriched mantle to shallow levels beneath a spreading centre close to a trench can explain the highly depleted compositions of Troodos glasses which have few modern equivalents, and possibly also the higher temperature of alteration of Troodos crust compared to oceanic crust (Alt and Teagle, 2000; Crawford et al., 1989; Falloon and Crawford, 1991). More detailed sampling of these young boninitic lavas are needed to test this model.

Ridge-trench-trench (RTT) and ridge-trench-transform (RTF) triple junctions may be stable plate tectonic configurations (McKenzie and Morgan, 1969) that can nevertheless propagate rapidly laterally, which could explain the similar age of many Tethyan "supra-subduction zone" ophiolites (Troodos, Oman, Kizildag – 91-95 Ma, (Mirdita-Vourinos-Crete-Pindos = 165-164-170-171 Ma) (Dilek and Flower, 2003; Dilek and Thy, 2009; Robertson, 2002). A spreading centre at an RTT or RTF triple junction will 'capture' the adjacent arc magmatism, which can explain the lack of overlying arc volcanics on Troodos and many other Tethyan ophiolites. Young, buoyant oceanic crust created on the over-riding plate close to a subduction zone will be particularly susceptible to obduction and preservation. Despite their

present rarity, these tectonic settings are therefore particularly efficient sites for SSZ ophiolite production and preservation.

Acknowledgments

We thank the Smithsonian Institution for providing electron microprobe standards, and Helene Brätz and Reiner Klemd for help with LA-ICP-MS analyses. We acknowledge Peter Michael for useful discussions, and Patrick Hoyer and Julia Bauer for help in the field. This research was funded by the Deutsche Forschungsgemeinschaft grant RE3020/11-1.

References

Alt, J. C., and Teagle, D. A., 2000, Hydrothermal alteration and fluid fluxes in ophiolites and oceanic crust: Special Papers-Geological Society of America, p. 273-282.

Bach, W., Hegner, E., and Erzinger, J., 1998, Chemical fluxes in the Tonga subduction zone: Evidence from the southern Lau Basin: Geophysical Research Letters, v. 25, no. 9, p. 1467-1470.

Beier, C., Brandl, P. A., Lima, S. M., and Haase, K. M., 2018, Tectonic control on the genesis of magmas in the New Hebrides arc (Vanuatu): Lithos, v. 312, p. 290-307.

Bézos, A., Escrig, S., Langmuir, C. H., Michael, P. J., and Asimow, P. D., 2009, Origins of chemical diversity of back- arc basin basalts: A segment- scale study of the Eastern Lau Spreading Center: Journal of Geophysical Research: Solid Earth, v. 114, no. B6.

Brandl, P. A., Regelous, M., Beier, C., O'Neill, H. S. C., Nebel, O., and Haase, K. M., 2016, The timescales of magma evolution at mid-ocean ridges: Lithos, v. 240, p. 49-68.

Casey, J., and Dewey, J., 1984, Initiation of subduction zones along transform and accreting plate boundaries, triple-junction evolution, and forearc spreading centres—implications for ophiolitic geology and obduction: Geological Society, London, Special Publications, v. 13, no. 1, p. 269-290.

Caulfield, J., Turner, S., Arculus, R., Dale, C., Jenner, F., Pearce, J., Macpherson, C., and Handley, H., 2012a, Mantle flow, volatiles, slab- surface temperatures and melting dynamics in the north Tonga arc–Lau back- arc basin: Journal of Geophysical Research: Solid Earth, v. 117, no. B11.

Caulfield, J., Turner, S. P., Smith, I., Cooper, L., and Jenner, G. A., 2012b, Magma evolution in the primitive, intra-oceanic Tonga arc: petrogenesis of basaltic andesites at Tofua volcano: Journal of petrology, v. 53, no. 6, p. 1197-1230.

Clube, T. M. M., Creer, K., and Robertson, A., 1985, Palaeorotation of the Troodos microplate, Cyprus: Nature, v. 317, no. 6037, p. 522.

Constantinou, G., 1995, Geological map of Cyprus: Geological Survey Department, Cyprus.

Cooper, L. B., Plank, T., Arculus, R. J., Hauri, E. H., Hall, P. S., and Parman, S. W., 2010, High- Ca boninites from the active Tonga Arc: Journal of Geophysical Research: Solid Earth, v. 115, no. B10.

Crawford, A. J., Beccaluva, L., and Serri, G., 1981, Tectono-magmatic evolution of the West Philippine-Mariana region and the origin of boninites: Earth and Planetary Science Letters, v. 54, no. 2, p. 346-356.

Crawford, A. J., Falloon, T., and Green, D., 1989, Classification, petrogenesis and tectonic setting of boninites: Boninites and related rocks, p. 1-49.

Danyushevsky, L. V., Sobolev, A. V., and Falloon, T. J., 1995, North Tongan high-Ca boninite petrogenesis: The role of Samoan plume and subduction zone-transform fault transition: Journal of Geodynamics, v. 20, no. 3, p. 219-241.

Dilek, Y., and Flower, M. F., 2003, Arc-trench rollback and forearc accretion: 2. A model template for ophiolites in Albania, Cyprus, and Oman: Geological Society, London, Special Publications, v. 218, no. 1, p. 43-68.

Dilek, Y., and Furnes, H., 2009, Structure and geochemistry of Tethyan ophiolites and their petrogenesis in subduction rollback systems: Lithos, v. 113, no. 1, p. 1-20.

Dilek, Y., and Thy, P., 2009, Island arc tholeiite to boninitic melt evolution of the Cretaceous Kizildag (Turkey) ophiolite: model for multi-stage early arc–forearc magmatism in Tethyan subduction factories: Lithos, v. 113, no. 1, p. 68-87.

Escrig, S., Bézos, A., Langmuir, C., Michael, P., and Arculus, R., 2012, Characterizing the effect of mantle source, subduction input and melting in the Fonualei Spreading Center, Lau Basin: Constraints on the origin of the boninitic signature of the back- arc lavas: Geochemistry, Geophysics, Geosystems, v. 13, no. 10.

Falloon, T. J., and Crawford, A. J., 1991, The petrogenesis of high-calcium boninite lavas dredged from the northern Tonga ridge: Earth and Planetary Science Letters, v. 102, no. 3-4, p. 375-394.

Falloon, T. J., Danyushevsky, L. V., Crawford, A. J., Meffre, S., Woodhead, J. D., and Bloomer, S. H., 2008, Boninites and adakites from the northern termination of the Tonga Trench: implications for adakite petrogenesis: Journal of Petrology, v. 49, no. 4, p. 697-715.

Falloon, T. J., Danyushevsky, L. V., Crawford, T. J., Maas, R., Woodhead, J. D., Eggins, S. M., Bloomer, S. H., Wright, D. J., Zlobin, S. K., and Stacey, A. R., 2007, Multiple mantle plume components involved in the petrogenesis of subduction- related lavas from the northern termination of the Tonga Arc and northern Lau Basin: Evidence from the geochemistry of arc and backarc submarine volcanics: Geochemistry, Geophysics, Geosystems, v. 8, no. 9.

Falloon, T. J., Green, D. H., and Crawford, A., 1987, Dredged igneous rocks from the northern termination of the Tofua magmatic arc, Tonga and adjacent Lau Basin: Australian Journal of Earth Sciences, v. 34, no. 4, p. 487-506.

Falloon, T. J., Green, D. H., and McCulloch, M., 1989, Petrogenesis of high-Mg and associated lavas from the north Tonga trench, p. 357-395.

Flower, M. F., and Levine, H. M., 1987, Petrogenesis of a tholeiite-boninite sequence from Ayios Mamas, Troodos ophiolite: evidence for splitting of a volcanic arc?: Contributions to Mineralogy and Petrology, v. 97, no. 4, p. 509-524.

Gale, A., Dalton, C. A., Langmuir, C. H., Su, Y., and Schilling, J. G., 2013, The mean composition of ocean ridge basalts: Geochemistry, Geophysics, Geosystems, v. 14, no. 3, p. 489-518.

Gass, I., 1968, Is the Troodos massif of Cyprus a fragment of Mesozoic ocean floor?: Nature, v. 220, p. 39-42.

Gass, I. G., MacLeod, C. J., Murton, B., Panayiotou, A., Simonian, K., and Xenophontos, C., 1994, The geological evolution of the Southern Troodos transform fault zone, Geological Survey Department, v. 9.

Hickey-Vargas, R., Yogodzinski, G., Ishizuka, O., McCarthy, A., Bizimis, M., Kusano, Y., Savov, I., and Arculus, R., 2018, Origin of depleted basalts during subduction initiation and early development of the Izu-Bonin-Mariana island arc: Evidence from IODP expedition 351 site U1438, Amami-Sankaku basin: Geochimica et Cosmochimica Acta, v. 229, p. 85-111.

Ishizuka, O., Hickey-Vargas, R., Arculus, R. J., Yogodzinski, G. M., Savov, I. P., Kusano, Y., McCarthy, A., Brandl, P. A., and Sudo, M., 2018, Age of Izu–Bonin–Mariana arc basement: Earth and Planetary Science Letters, v. 481, p. 80-90.

Ishizuka, O., Kimura, J.-I., Li, Y. B., Stern, R. J., Reagan, M. K., Taylor, R. N., Ohara, Y., Bloomer, S. H., Ishii, T., and Hargrove, U. S., 2006, Early stages in the evolution of Izu–Bonin arc volcanism: New age, chemical, and isotopic constraints: Earth and Planetary Science Letters, v. 250, no. 1, p. 385-401.

Ishizuka, O., Tani, K., and Reagan, M. K., 2014, Izu-Bonin-Mariana forearc crust as a modern ophiolite analogue: Elements, v. 10, no. 2, p. 115-120.

Ishizuka, O., Tani, K., Reagan, M. K., Kanayama, K., Umino, S., Harigane, Y., Sakamoto, I., Miyajima, Y., Yuasa, M., and Dunkley, D. J., 2011, The timescales of subduction initiation and subsequent evolution of an oceanic island arc: Earth and Planetary Science Letters, v. 306, no. 3, p. 229-240.

Karsten, J., Klein, E., and Sherman, S., 1996, Subduction zone geochemical characteristics in ocean ridge basalts from the southern Chile Ridge: implications of modern ridge subduction systems for the Archean: Lithos, v. 37, no. 2-3, p. 143-161.

Keller, N. S., Arculus, R. J., Hermann, J., and Richards, S., 2008, Submarine back- arc lava with arc signature: Fonualei Spreading Center, northeast Lau Basin, Tonga: Journal of Geophysical Research: solid earth, v. 113, no. B8.

König, S., Münker, C., Schuth, S., Luguet, A., Hoffmann, J. E., and Kuduon, J., 2010, Boninites as windows into trace element mobility in subduction zones: Geochimica et Cosmochimica Acta, v. 74, no. 2, p. 684-704.

Langmuir, C., Bezos, A., Escrig, S., and Parman, S., 2006, Chemical systematics and hydrous melting of the mantle in back- arc basins: Back-Arc Spreading Systems: Geological, Biological, Chemical, and Physical Interactions, p. 87-146.

Le Bas, M., 2000, IUGS reclassification of the high-Mg and picritic volcanic rocks: Journal of Petrology, v. 41, no. 10, p. 1467-1470.

Le Voci, G., Davies, D., Goes, S., Kramer, S. C., and Wilson, C. R., 2014, A systematic 2- D investigation into the mantle wedge's transient flow regime and thermal structure: Complexities arising from a hydrated rheology and thermal buoyancy: Geochemistry, Geophysics, Geosystems, v. 15, no. 1, p. 28-51.

Maffione, M., Hinsbergen, D. J., Gelder, G. I., Goes, F. C., and Morris, A., 2017, Kinematics of Late Cretaceous subduction initiation in the Neo- Tethys Ocean reconstructed from ophiolites of Turkey, Cyprus, and Syria: Journal of Geophysical Research: Solid Earth, v. 122, no. 5, p. 3953-3976.

McDonough, W. F., and Sun, S.-S., 1995, The composition of the Earth: Chemical geology, v. 120, no. 3, p. 223-253.
McKenzie, D. P., and Morgan, W., 1969, Evolution of triple junctions: Nature, v. 224, no. 5215, p. 125.
Miyashiro, A., 1974, Volcanic rock series in island arcs and active continental margins: American Journal of Science, v. 274, no. 4, p. 321-355.
Moores, E., Robinson, P. T., Malpas, J., and Xenophonotos, C., 1984, Model for the origin of the Troodos massif, Cyprus, and other mideast ophiolites: Geology, v. 12, no. 8, p. 500-503.
Moores, E., and Vine, F., 1971, The Troodos Massif, Cyprus and other ophiolites as oceanic crust: evaluation and implications: Philosophical Transactions of the Royal Society of London A: Mathematical, Physical and Engineering Sciences, v. 268, no. 1192, p. 443-467.
Mukasa, S. B., and Ludden, J. N., 1987, Uranium-lead isotopic ages of plagiogranites from the Troodos ophiolite, Cyprus, and their tectonic significance: Geology, v. 15, no. 9, p. 825-828.
Osozawa, S., Shinjo, R., Lo, C.-H., Jahn, B.-m., Hoang, N., Sasaki, M., Ishikawa, K. i., Kano, H., Hoshi, H., and Xenophontos, C., 2012, Geochemistry and geochronology of the Troodos ophiolite: An SSZ ophiolite generated by subduction initiation and an extended episode of ridge subduction?: Lithosphere, v. 4, no. 6, p. 497-510.
Pearce, J., 1975, Basalt geochemistry used to investigate past tectonic environments on Cyprus: Tectonophysics, v. 25, no. 1-2, p. 41-67.
Pearce, J., and Robinson, P., 2010, The Troodos ophiolitic complex probably formed in a subduction initiation, slab edge setting: Gondwana Research, v. 18, no. 1, p. 60-81.
Pearce, J. A., Ernewein, M., Bloomer, S. H., Parson, L. M., Murton, B. J., and Johnson, L. E., 1994, Geochemistry of Lau Basin volcanic rocks: influence of ridge segmentation and arc proximity: Geological Society, London, Special Publications, v. 81, no. 1, p. 53-75.
Pearce, J. A., Lippard, S., and Roberts, S., 1984, Characteristics and tectonic significance of supra-subduction zone ophiolites: Geological Society, London, Special Publications, v. 16, no. 1, p. 77-94.
Pearce, J. A., Reagan, M. K., Petronotis, K., Morgan, S., Almeev, R., Avery, A. J., Carvallo, C., Chapman, T., Christeson, G. L., and Ferré, E. C., 2015, Izu-Bonin-Mariana fore arc: Testing subduction initiation and ophiolite models by drilling the outer Izu-Bonin-Mariana fore arc; 30 July–29 September 2014: Integrated Ocean Drilling Program: Preliminary Reports, v. 352.
Peate, D. W., Kokfelt, T. F., Hawkesworth, C. J., Van Calsteren, P. W., Hergt, J. M., and Pearce, J. A., 2001, U-series isotope data on Lau Basin glasses: The role of subduction-related fluids during melt generation in back-arc basins: Journal of Petrology, v. 42, no. 8, p. 1449-1470.
Peate, D. W., Pearce, J. A., Hawkesworth, C. J., Colley, H., Edwards, C. M., and Hirose, K., 1997, Geochemical variations in Vanuatu arc lavas: the role of subducted material and a variable mantle wedge composition: Journal of Petrology, v. 38, no. 10, p. 1331-1358.
Rautenschlein, M., Jenner, G., Hertogen, J., Hofmann, A., Kerrich, R., Schmincke, H.-U., and White, W., 1985, Isotopic and trace element composition of volcanic glasses from the Akaki Canyon, Cyprus: implications for the origin of the Troodos ophiolite: Earth and Planetary Science Letters, v. 75, no. 4, p. 369-383.

Reagan, M. K., Ishizuka, O., Stern, R. J., Kelley, K. A., Ohara, Y., Blichert- Toft, J., Bloomer, S. H., Cash, J., Fryer, P., and Hanan, B. B., 2010, Fore- arc basalts and subduction initiation in the Izu- Bonin- Mariana system: Geochemistry, Geophysics, Geosystems, v. 11, no. 3.

Reagan, M. K., Pearce, J. A., Petronotis, K., Almeev, R. R., Avery, A. J., Carvallo, C., Chapman, T., Christeson, G. L., Ferré, E. C., and Godard, M., 2017, Subduction initiation and ophiolite crust: new insights from IODP drilling: International Geology Review, v. 59, no. 11, p. 1439-1450.

Regelous, M., Haase, K., Freund, S., Keith, M., Weinzierl, C., Beier, C., Brandl, P., Endres, T., and Schmidt, H., 2014, Formation of the Troodos Ophiolite at a triple junction: Evidence from trace elements in volcanic glass: Chemical Geology, v. 386, p. 66-79.

Resing, J. A., Rubin, K. H., Embley, R. W., Lupton, J. E., Baker, E. T., Dziak, R. P., Baumberger, T., Lilley, M. D., Huber, J. A., and Shank, T. M., 2011, Active submarine eruption of boninite in the northeastern Lau Basin: Nature Geoscience, v. 4, no. 11, p. 799-806.

Robertson, A. H., 2002, Overview of the genesis and emplacement of Mesozoic ophiolites in the Eastern Mediterranean Tethyan region: Lithos, v. 65, no. 1, p. 1-67.

Robinson, P. T., Malpas, J., Xenophontos, C., Dilek, Y., and Newcomb, S., 2003, The Troodos massif of Cyprus: Its role in the evolution of the ophiolite concept: Special papers-Geological Society of America, p. 295-308.

Robinson, P. T., Melson, W. G., O'Hearn, T., and Schmincke, H.-U., 1983, Volcanic glass compositions of the Troodos ophiolite, Cyprus: Geology, v. 11, no. 7, p. 400-404.

Sharaskin, A. Y., Karpenko, S., Ljalikov, A., Zlobin, S., and Balashov, Y., 1983, Correlated 143Nd/144Nd and 87Sr/86Sr data on boninites from Mariana and Tonga arcs: Ofioliti, v. 8, no. 3, p. 431-438.

Sigurdsson, I., Kamenetsky, V., Crawford, A., Eggins, S., and Zlobin, S., 1993, Primitive island arc and oceanic lavas from the Hunter ridge-Hunter fracture zone. Evidence from glass, olivine and spinel compositions: Mineralogy and Petrology, v. 47, no. 2-4, p. 149-169.

Stern, R. J., Reagan, M., Ishizuka, O., Ohara, Y., and Whattam, S., 2012, To understand subduction initiation, study forearc crust: To understand forearc crust, study ophiolites: Lithosphere, v. 4, no. 6, p. 469-483.

Syracuse, E. M., and Abers, G. A., 2006, Global compilation of variations in slab depth beneath arc volcanoes and implications: Geochemistry, Geophysics, Geosystems, v. 7, no. 5.

Whattam, S. A., and Stern, R. J., 2011, The ‘subduction initiation rule’: a key for linking ophiolites, intra-oceanic forearcs, and subduction initiation: Contributions to Mineralogy and Petrology, v. 162, no. 5, p. 1031-1045.

Woelki, D., Regelous, M., Haase, K. M., Romer, R. H., and Beier, C., 2018, Petrogenesis of boninitic lavas from the Troodos Ophiolite, and comparison with Izu–Bonin–Mariana fore-arc crust: Earth and Planetary Science Letters, v. 498, p. 203-214.

Figure captions

Figure 1. Simplified geological map of the Troodos Ophiolite (modified from Osozawa et al. (2012)), showing sample locations (grey dots), profiles through the extrusive series (black lines) and the three areas (NM, SWM, SEM) defined on the basis of trace element composition.

Figure 2. Major element variations (MgO, SiO_2 and TiO_2) in volcanic glasses from the Troodos Ophiolite. Data are from this study, Akaki (Regelous et al., 2014) and Parekklisia (Woelki et al., 2018). Fields defined for boninites (BON) are based on the classification of Le Bas (2000). Based on this classification, boninites are restricted to the SWM and SEM glasses.

Figure 3. Trace element composition of Troodos glasses normalized to N-MORB (McDonough and Sun, 1995). All NM, SWM and SEM glasses (data from this study and Regelous et al. (2014); Woelki et al. (2018)) are enriched in fluid mobile elements Cs, Rb, Ba, U, Pb and Sr, compared to less mobile elements of similar incompatibility. The mean Troodos boninite composition is based on 142 analyses from this work and from Woelki et al. (2018). Note the relatively high Zr and Hf compared to Sm and Eu in IBM boninites (Reagan et al., 2010), compared to boninites from Troodos and from young back-arc (Falloon and Crawford, 1991; Falloon et al., 2008; Falloon et al., 2007; Falloon et al., 1989) and arc (Cooper et al., 2010) settings.

Figure 4. A. Variation in glass composition with distance from the lava-sediment boundary as determined from the geological map of Cyprus (Constantinou, 1995) for seven different sections through the Troodos lava sequence. The bar represents mean composition for each section. Note

that most sections show no systematic geochemical variation with relative stratigraphic age. Instead, glasses from the northern margin (NM) have higher Zr/Yb ratios than glasses from the southern margin (SWM, SEM), indicating that those from the northern margin were derived from a less depleted mantle source. B. Box-whisker plot of Ba/Ce ratios for glasses from the seven sections, with whiskers extended to most extreme data points. Glasses from the southern margin (SWM, SEM) have higher Ba/Ce than glasses from the northern margin.

Figure 5. Variation of Ce/Pb with Zr/Yb in Troodos glasses, compared with lavas from (A) the IBM fore-arc (Hickey-Vargas et al., 2018; Ishizuka et al., 2018; Ishizuka et al., 2011; Reagan et al., 2010), and (B) the Tonga-Lau arc – back-arc system. Troodos data are from Regelous et al. (2014); Woelki et al. (2018) and this study. (A) Troodos NM glasses overlap in composition with some IBM lavas, but extend to far lower Zr/Yb ratios. Troodos glasses define positive correlations between Zr/Yb and Ce/Pb, in contrast to the negative correlation for IBM fore-arc lavas. (B) The Zr/Yb and Ce/Pb ratios of Troodos NM glasses overlap with Fonualei Rift back-arc lavas (Escrig et al., 2012) (dashed field) indicating similar degree of mantle depletion and subduction enrichment. The Ce/Pb and Zr/Yb ratios of SWM and SEM glasses partly overlap with Tofua island arc lavas (Caulfield et al., 2012b), but extend to lower Ce/Pb and Zr/Yb. Data for Eastern Lau and Central Lau Spreading Centre lavas from Bézos et al. (2009); Pearce et al. (1994); Peate et al. (2001), MORB data from Jenner and O'Neill, 2012, Valu Fa Ridge data are from Bach et al. (1998), Tonga boninite data are from Cooper et al. (2010); Falloon and Crawford (1991); Falloon et al. (2008); Falloon et al. (2007); Falloon et al. (1989).

Figure 6. Distance to arc (km) plotted against Zr/Yb and Ce/Pb ratios of Tonga – Lau Basin glasses. Distance to arc in the Tonga arc-back-arc system measured by GeoMapApp® application (http://www.geomapapp.org/). Mantle wedge depletion (decreasing Zr/Yb) and subduction component enrichment (decreasing Ce/Pb) increases with decreasing distance to the arc for the Tonga back-arc system (Bach et al., 1998; Bézos et al., 2009; Escrig et al., 2012; Pearce et al., 1994; Peate et al., 1997). The boxes of Troodos glasses represent box-whisker plots extended to the most extreme values and compared distances of the Fonualei spreading centre (Escrig et al., 2012). The NM glasses overlap with Fonualei Spreading centre lavas, which are 25 – 75 km away from the active arc. Compositional field of the Troodos NM, SWM and SEM indicate a distance less than 75 km to the "arc" position.

Figure 7. Ti_8 and Fe_8 (TiO_2 and FeO contents fractionation corrected to MgO = 8 wt%, based on the liquid line of descent) of the Troodos glasses. Only glasses >5 wt% MgO are used for correction. Data are from this study and Regelous et al. (2014); Woelki et al. (2018). Shown for comparison are global MORB (Gale et al., 2013), Fonualei Spreading Centre (Escrig et al., 2012) and ELSC glasses (grey field) (Bézos et al., 2009). Troodos glasses overlap with back-arc lava trends of the ELSC and Fonualei spreading centre towards lower Ti_8 and Fe_8 values. Grey symbols for melting conditions are from Langmuir et al. (2006).

Figure 8. Inferred position and orientation of the former subduction zone beneath the Troodos Ophiolite, with the Troodos Ophiolite rotated 90° clockwise to its orientation at 91 Ma. Red dashed lines indicate approximate distance to slab surface inferred from comparison with global arc and back-arc systems including the Tonga-Lau system (Caulfield et al., 2012a; Escrig et al.,

2012; Keller et al., 2008; Syracuse and Abers, 2006). Blue lines are parallel to the former Troodos spreading axis, with arrows indicating spreading direction on the basis of sheeted dyke orientations (Maffione et al., 2017). Black line represents the Arakapas Fault Zone (Gass et al., 1994).

Figure 1

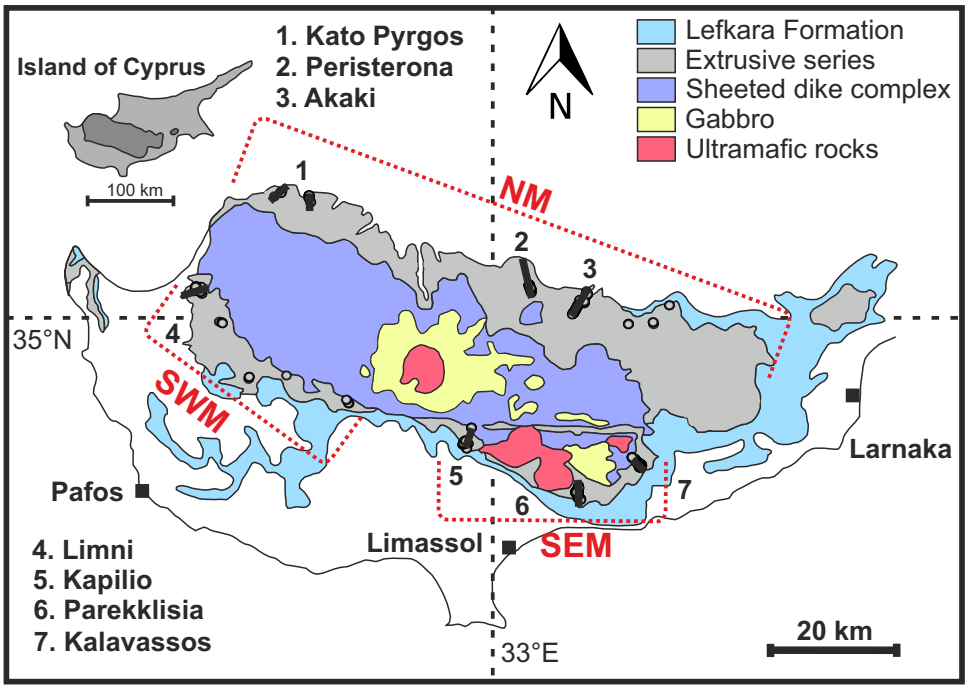
Island of Cyprus
100 km
1. Kato Pyrgos
2. Peristerona
3. Akaki
N
Lefkara Formation
Extrusive series
Sheeted dike complex
Gabbro
Ultramafic rocks
NM
SWM
SEM
35°N
33°E
Pafos
Limassol
Larnaka
4. Limni
5. Kapilio
6. Parekklisia
7. Kalavassos
20 km

Figure 2

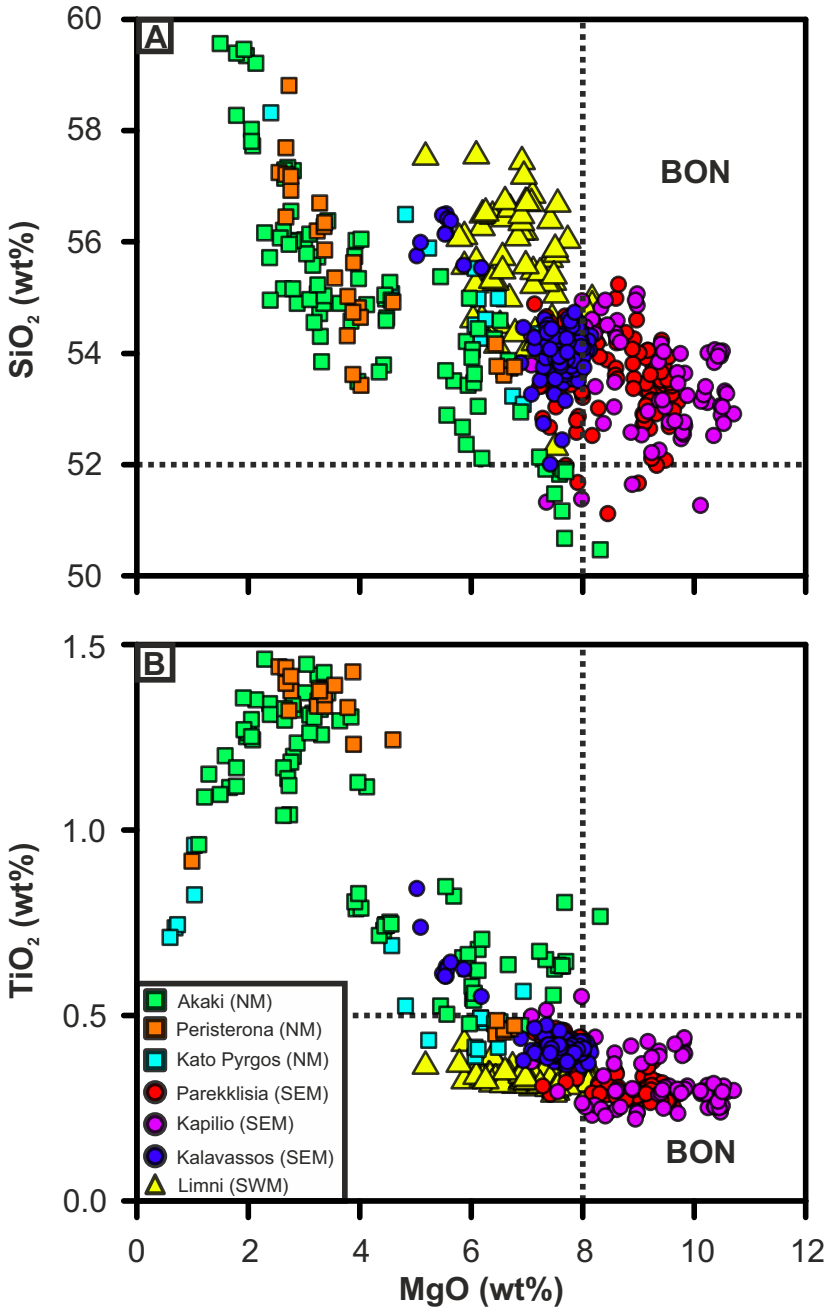
A
B
BON
BON
SiO2 (wt%)
TiO2 (wt%)
MgO (wt%)
60
58
56
54
52
50
1.5
1.0
0.5
0.0
0
2
4
6
8
10
12
Akaki (NM)
Peristerona (NM)
Kato Pyrgos (NM)
Parekklisia (SEM)
Kapilio (SEM)
Kalavassos (SEM)
Limni (SWM)

Figure 3

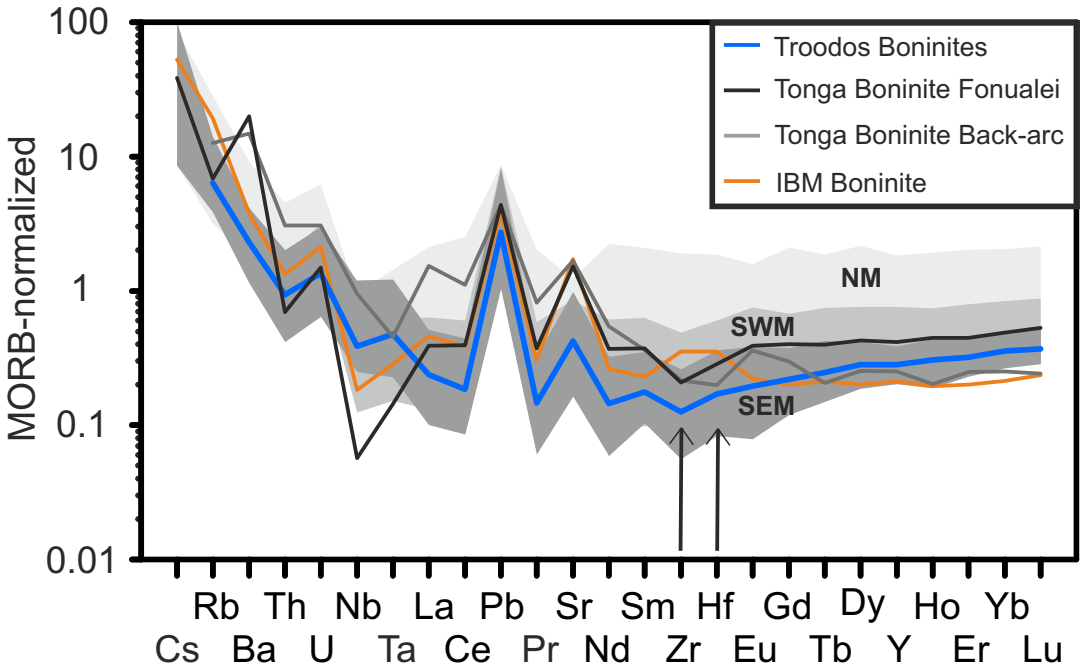
100
10
1
0.1
0.01
MORB-normalized
Troodos Boninites
Tonga Boninite Fonualei
Tonga Boninite Back-arc
IBM Boninite
NM
SWM
SEM
Cs Rb Ba Th U Nb Ta La Ce Pb Pr Sr Nd Sm Zr Hf Eu Gd Tb Dy Y Ho Er Yb Lu

Figure 4

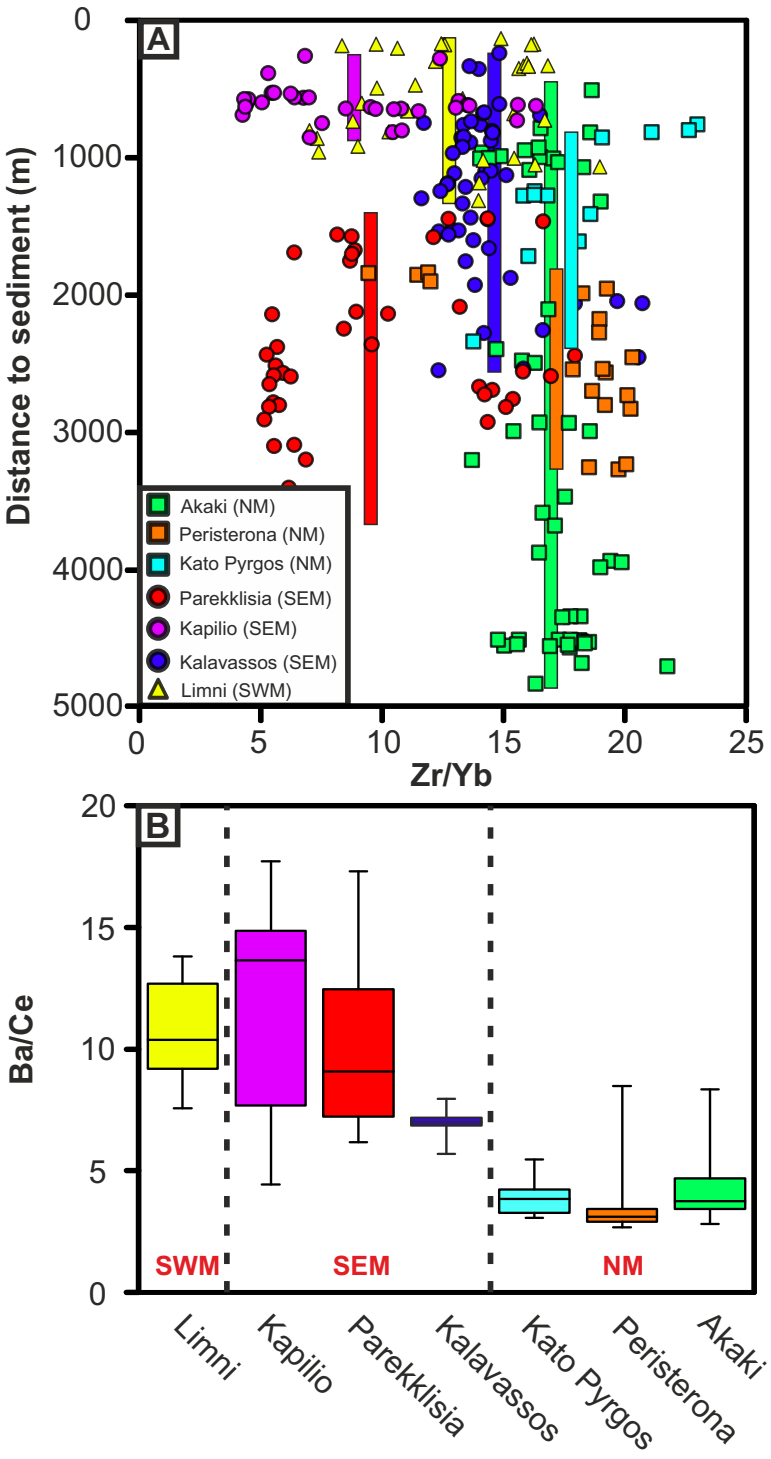
A
Distance to sediment (m)
0
1000
2000
3000
4000
5000
0
5
10
15
20
25
Zr/Yb
Akaki (NM)
Peristerona (NM)
Kato Pyrgos (NM)
Parekklisia (SEM)
Kapilio (SEM)
Kalavassos (SEM)
Limni (SWM)
B
Ba/Ce
20
15
10
5
0
SWM
SEM
NM
Limni
Kapilio
Parekklisia
Kalavassos
Kato Pyrgos
Peristerona
Akaki

Figure 5

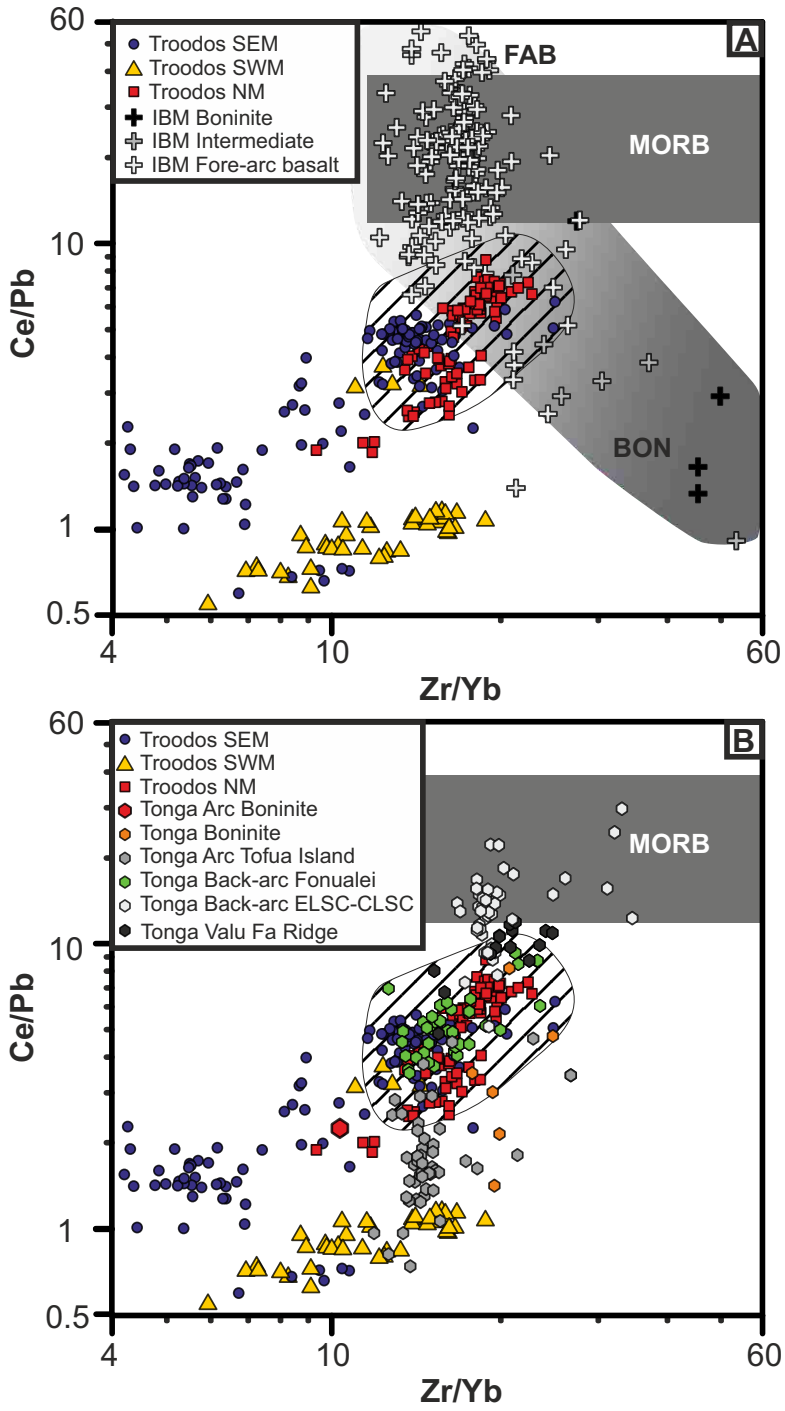
A
Troodos SEM
Troodos SWM
Troodos NM
IBM Boninite
IBM Intermediate
IBM Fore-arc basalt
FAB
MORB
BON
Ce/Pb
Zr/Yb
60
10
1
0.5
4
10
60
B
Troodos SEM
Troodos SWM
Troodos NM
Tonga Arc Boninite
Tonga Boninite
Tonga Arc Tofua Island
Tonga Back-arc Fonualei
Tonga Back-arc ELSC-CLSC
Tonga Valu Fa Ridge
MORB
Ce/Pb
Zr/Yb

Figure 6

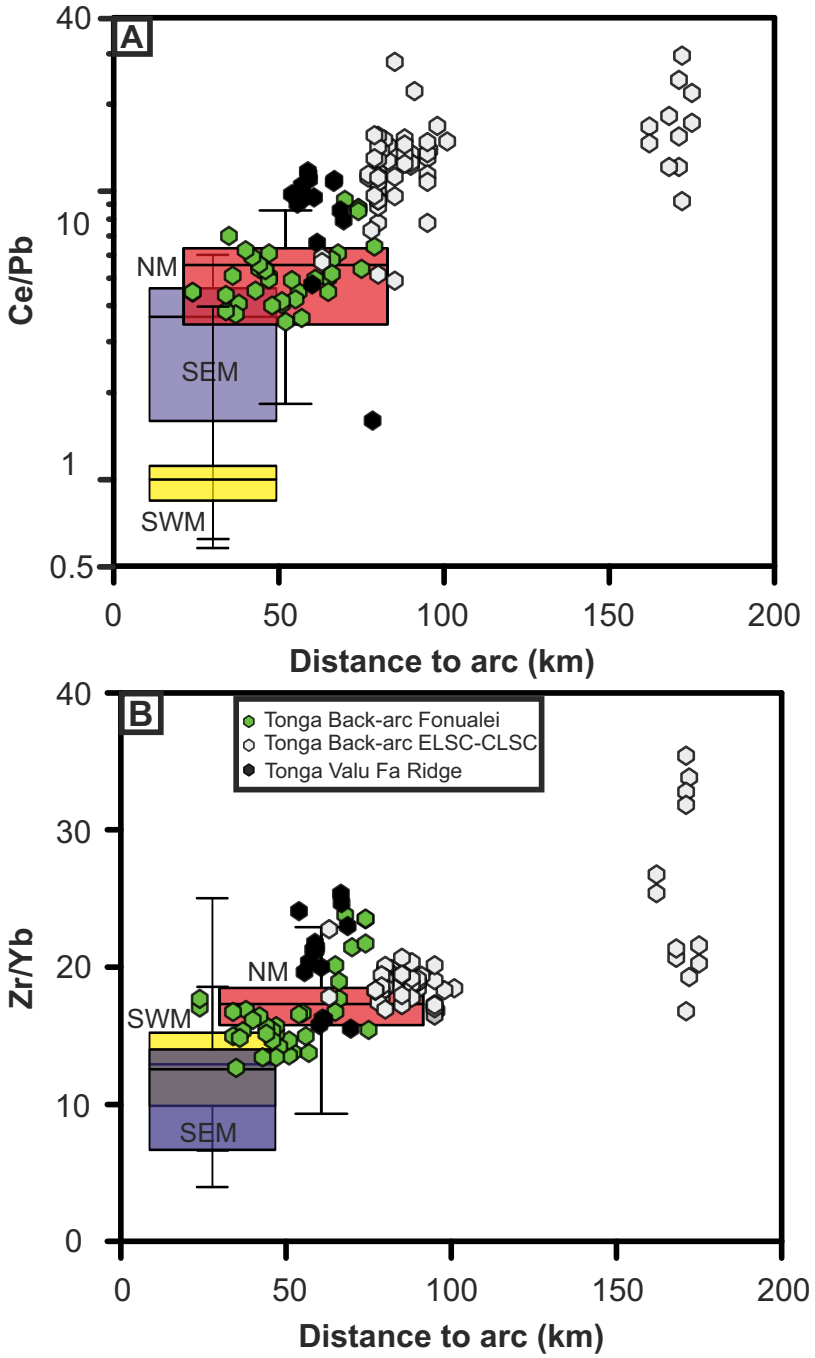
A
Ce/Pb
40
10
1
0.5
NM
SEM
SWM
0
50
100
150
200
Distance to arc (km)
B
Tonga Back-arc Fonualei
Tonga Back-arc ELSC-CLSC
Tonga Valu Fa Ridge
Zr/Yb
40
30
20
10
0
NM
SWM
SEM
0
50
100
150
200
Distance to arc (km)

Figure 7

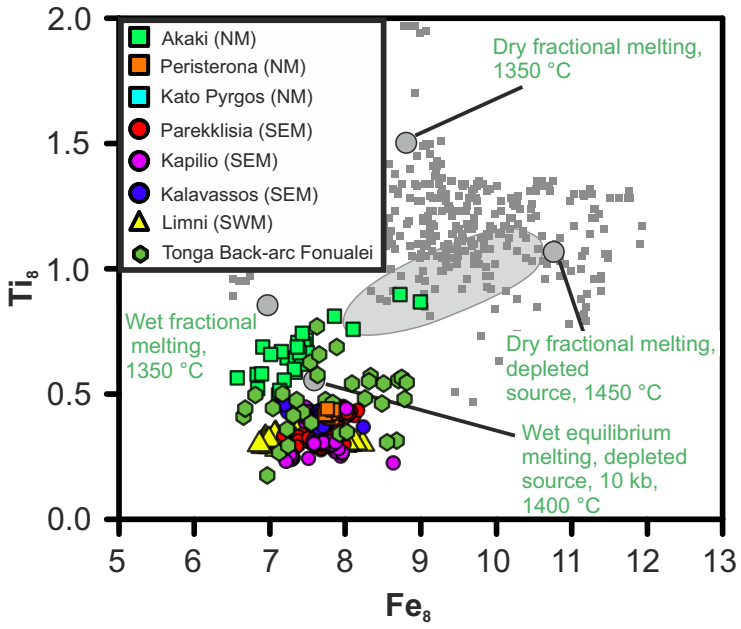
Akaki (NM)
Peristerona (NM)
Kato Pyrgos (NM)
Parekklisia (SEM)
Kapilio (SEM)
Kalavassos (SEM)
Limni (SWM)
Tonga Back-arc Fonualei
Dry fractional melting, 1350 °C
Wet fractional melting, 1350 °C
Dry fractional melting, depleted source, 1450 °C
Wet equilibrium melting, depleted source, 10 kb, 1400 °C
Ti8
Fe8
2.0
1.5
1.0
0.5
0.0
5
6
7
8
9
10
11
12
13

Figure 8

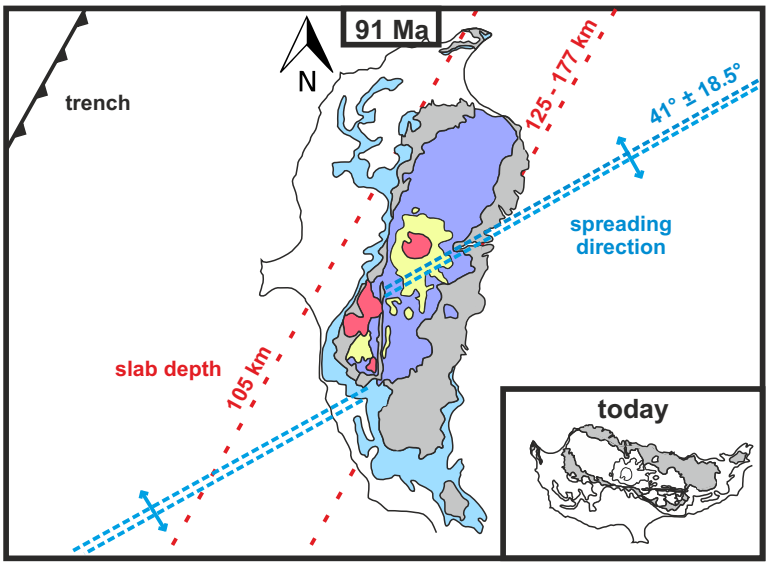
91 Ma
N
trench
125 - 177 km
41° ± 18.5°
spreading direction
slab depth
105 km
today

Figure S1

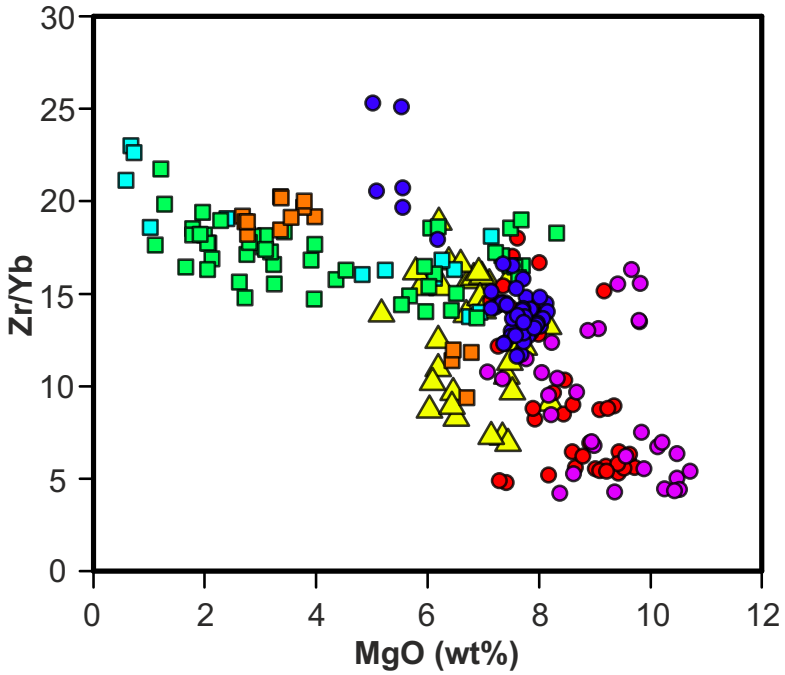

Figure S1. Variation of Zr/Yb with MgO (wt%) for Troodos glasses. There is no systematic variation of Zr/Yb with MgO for each individual group, indicating source variation rather than crystal fractionation or crustal assimilation.

supplemental table 1

Click here to download Table: supplemental table S1.xlsx

TABLE S1. MAJOR (WT%) AND TRACE ELEMENT (PPM) COMPOSITION OF TROOD

Sample #	IGSN sample #	Rock Type	Locality
CY16-GLASS-1	IEGZN0001	Tholeiite	Limni
CY16-GLASS-2	IEGZN0002	Tholeiite	Limni
CY16-GLASS-3	IEGZN0003	Tholeiite	Limni
CY16-GLASS-11	IEGZN0004	Tholeiite	Limni
CY16-GLASS-12	IEGZN0005	Tholeiite	Limni
CY16-GLASS-14	IEGZN0006	Boninite	Limni
CY16-GLASS-19	IEGZN0007	Tholeiite	Limni
CY16-GLASS-20	IEGZN0008	Tholeiite	Limni
CY16-GLASS-21	IEGZN0009	Tholeiite	Limni
CY16-GLASS-23	IEGZN0010	Tholeiite	Limni
CY16-GLASS-24	IEGZN0011	Tholeiite	Limni
CY16-GLASS-25	IEGZN0012	Tholeiite	Limni
CY16-GLASS-26	IEGZN0013	Tholeiite	Limni
CY16-GLASS-27	IEGZN0014	Tholeiite	Limni
CY16-GLASS-28	IEGZN0015	Tholeiite	Limni
CY16-GLASS-29	IEGZN0016	Boninite	Limni
CY16-GLASS-30	IEGZN0017	Boninite	Limni
Cy16-GLASS-31	IEGZN0018	Boninite	Limni
CY16-GLASS-32	IEGZN0019	Tholeiite	Limni
CY16-GLASS-33	IEGZN0020	Tholeiite	Limni
CY16-GLASS-34	IEGZN0021	Tholeiite	Limni
CY16-GLASS-35	IEGZN0022	Tholeiite	Limni
CY16-GLASS-36	IEGZN0023	Tholeiite	Limni
CY16-GLASS-37	IEGZN0024	Tholeiite	Limni
CY16-GLASS-38	IEGZN0025	Tholeiite	Limni
CY16-GLASS-39	IEGZN0026	Tholeiite	Limni
CY16-GLASS-40	IEGZN0027	Tholeiite	Limni
CY16-GLASS-42	IEGZN0028	Tholeiite	Limni
CY16-GLASS-43	IEGZN0029	Tholeiite	Limni
CY16-GLASS-44	IEGZN0030	Tholeiite	Limni
CY1601	IEGZN0031	Boninite	Limni
CY1603	IEGZN0032	Tholeiite	Limni
CY1604	IEGZN0033	Tholeiite	Limni
CY1606	IEGZN0034	Tholeiite	Limni
CY1608	IEGZN0035	Tholeiite	Limni
CY1610	IEGZN0036	Tholeiite	Limni
CY1611	IEGZN0037	Tholeiite	Limni
CY1612	IEGZN0038	Tholeiite	Limni
CY1613	IEGZN0039	Tholeiite	Limni
CY1614	IEGZN0040	Tholeiite	Limni
CY1616	IEGZN0041	Tholeiite	Limni
CY1617	IEGZN0042	Tholeiite	Limni
CY1619	IEGZN0043	Tholeiite	Limni
CY1620	IEGZN0044	Tholeiite	Limni
CY1621	IEGZN0045	Tholeiite	Limni
CY1622	IEGZN0046	Tholeiite	Limni
CY1623	IEGZN0047	Boninite	Limni